Analysis of epoxy damage during the double cantilever beam test

Mariusz Kłonica[1]*, Sylwester Samborski[1], Jakub Skoczylas[1], Jakub Paśnik[1]

[1] Faculty of Mechanical Engineering, Lublin University of Technology, ul. Nadbystrzycka 36, 20-618 Lublin, Poland
* Corresponding author's e-mail: m.klonica@pollub.pl

ABSTRACT

In the study, acoustic emission (AE) technique was applied to monitor polymer failures. Specimens produced of two aluminum flat bars bonded together with a thick layer of cured epoxy resin were subjected to double cantilever beam (DCB) test. Epidian 5 epoxy resin cured with PAC curing agent as well as Epidian 53 epoxy resin cured with Z1 curing agent were used as adhesives. However, a special procedure of specimens preparation was needed which was elaborated by authors after preliminary research including aditional analysis of surface roughness parameters and surface free energy of aluminum flat bars. Acoustic emission system was then used to register AE signal parameters during fracture test: frequency of elastic waves emitted inside the material, number of hits (event), number of counts, energy and amplitude. Next, the obtained AE parameters were deeply analyzed and compared to the results of mechanical test and authors' previously conducted examinations. Moreover, a special emphasis was put on applicability of wawelet transform (WT) as well as numerical simulation for fracture analysis was conducted.

Keywords: acoustic emission, DCB test, epoxy resin, surface free energy.

INTRODUCTION

AE has become one of the most promising techniques applied in health monitoring [1–3] and failure detection [4–6]. The main advantage of this method is that it let to indicate the onset of propagation at the beginning of failure [7–9]. Acoustic waves are connected with strain energy release and emitted as a result of material failure [10]. During crack propagation the energy continues to release [11]. However, AE refers to frequencies over 20 kHz and up to 1 MHz so that they cannot be heard by humans [4]. Based on the literature AE is one of the most reliable techniques to monitor damage happened inside various types of polymer materials during different kinds of fracture tests [12–14]. AE technique is widely used in the case of various specimens, e.g. made of laminates [8, 9] or adhesively bonded metals [14]. The range of frequencies of the emitted elastic waves are different in case of various materials and conditions and may also vary in case of damage types occurred [1, 3, 13, 15–17].

Based on the literature many defects occurred inside materials can be referred to specific ranges of AE frequencies, e.g. 63 kHz was correlated with matrix cracking whereas 213 kHz was assigned to fiber breakage in glass/epoxy laminates [4].

Acoustic emission signals are registered using piezoelectric sensors due to conversion of stress waves released inside material. This signals are known as hits (events) [1, 15]. Number of hits is one of the most important AE parameters. Other useful parameters are: number of counts, peak amplitude value, rise time (RT), duration, threshold, AE frequency (f_{AE}) and AE energy (E_{AE}). Threshold need to be set in order to distinguish the signal from noise. Counts mean the value of times the threshold is crossed by a waveform while amplitude is rising, as indicated in Figure 1. AE energy means the energy registered during elastic waves release. Rise time is a period of time during which the amplitude rises until it gains its maximum value. Time duration is a time between the first and the last time when a waveform meets the threshold line [6]. Moreover,

amplitude is described as the maximum amplitude of a hit [18].

AE analysis is based on applying useful signal analysis tools such as fast fourier transform (FFT) and WT, which helps to interpret the results. FFT let to decompose the obtained signal into sine and cosine functions in frequency domain showing signal components frequencies and amplitudes [19]. However, no information is given by FFT on when in time a particular frequency of event occurred. While FFT is based on using analysis of waves, WT analyzes wavelets which are "small waves" with their energy focused in time [11]. Hence, WT is a solution to get the more accurate information because it is also localized in time [20, 21]. WT has become an important analysis tool used for structure of signal analysis [22]. Moreover it can be also applied to inhomogeneous functions [11].

Cured epoxy resins are applied in contemporary engineering as coatings or adhesives. Moreover, they are also widely used as fiber reinforced polymer (FRP) composites' matrices [23, 24]. It is crucial to evaluate the mechanical behavior of cured epoxies because they are generally quite brittle and have relatively low fracture toughness [25, 26]. Damage monitoring, especially using AE can help to detect damage just after it initiates and prevent further catastrophic failure. Although cured epoxy resins have some disadvantages such as their brittleness they are characterized as materials with excellent adhesive properties, tolerant to changing environmental conditions, resistant to corrosion as well as to different chemical conditions [27–31].

The main goal of the prezented work was to test adhesive material during DCB test, which is a mode I fracture test. However, it would not be possible to open a specimen using testing machine if a specimen is made of adhesive material only. Thus, aluminum flat bars were used as a stiffening elements which helps to conduct the experiment. Note that bonded joints between test material and aluminum flat bar surface must be strong enough. However, the aim of the research is to test adhesive layer only, not the adhesive-flat bar joint. Hence, the adhesive layer was quite
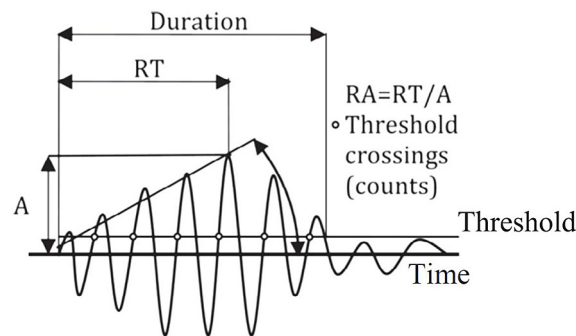
Figure 1. Schematic view of acoustic emission signal and its parameters [2]
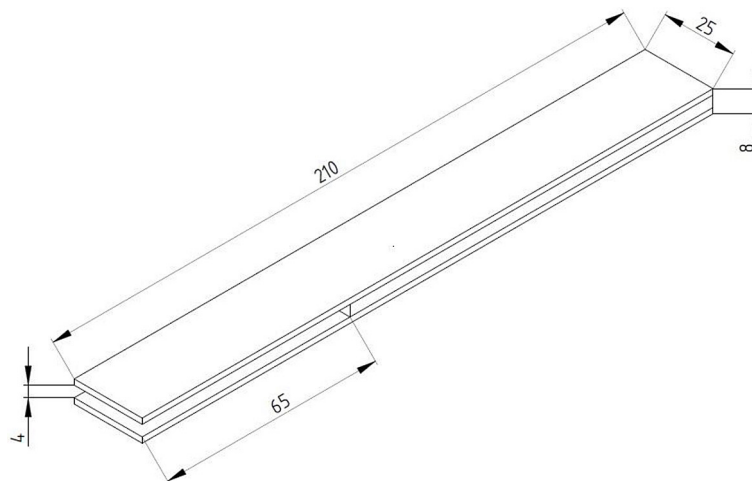
Figure 2. Schematic view of DCB specimen

thick and stiffening elements (aluminum flat bars) were just used to support the test.

The paper presents an adaptation of ASTM D5528-13 Standard [32] to monitor polymer failures. Figure 2 shows a schematic 3D model of a specimen used for DCB testing. All dimensions are indicated. During the test AE was used to register the parameters of elastic waves.

In the paper [33] the technological aspects of the joint were discussed, in particular the method of controlling the gap and the various adhesive products used to join the parts. The design process consisted of determining the geometry of the adhesive bond basing both on available adhesive models as well as real life testing and the technological solutions applied.

EXPERIMENTAL PROCEDURE

Specimens preparation

The paper investigates the AE signals emitted during fracture of DCB specimens made of two layers of aluminum flat bars and internal epoxy layer placed between them. Specimens dimensions (in relation to Fig. 2) were as follows: specimen length l = 210 mm, pre-crack length a = 65 mm, width b = 25 mm, thickness h = 8 mm, wherein the thickness of cured epoxy resin was equal to 4 mm. Aluminum flat bars with a thickness of 2 mm made of alloy EN-AW 6060/6063 with modulus of elasticity and modulus of rigidity equal to 69 GPa and 26 GPa, respectively were used to prepare the specimens. During the test it was crucial to make the crack propagates directly inside of polymer and prevent the propagation goes near or into the surface of aluminum flat bar. To ensure that adhesive properties of the flat bar

surface are good enough, before use their interior sides were firstly treated by sand paper P150, then sandblasted and finally degreased three times using Loctite 7063.

Two kinds of epoxy materials were fabricated at laboratory conditions. Material symbols (I, II) and material designations were assigned and given in Table 1. Two types of epoxy resins as well as two types of curing agents were selected: Epidian 53 epoxy resin (E53) cured with Z1 curing agent and Epidian 5 epoxy resin (E5) cured with PAC curing agent. In both cases the proper amount of curing agent was added to a weighed epoxy resin, which was expressed as a percentage of a total weight of resin. According to that, Z1 curing agent was added to E53 in the amount of 10% of a total weight of E53 wheras PAC curing agent was added to E5 in the amount of 60% of a total weight of E5. In both cases the mixtures of epoxy resin and curing agent were prepared by the same technique. Firstly, a three-minute blending process was conducted using a mechanical mixer with rpm set to 1130. Then a vacuum chamber with a pump was used to remove the air bubbles from the mixture. After this the blend was ready to fill the space between aluminum flat bars.

In order to prepare DCB specimens with a layer of cured epoxy resin thick on 4 mm and long on l-a = 145 mm (as indicated in Fig. 2) a specific steel counter-form was produced, as presented in Fig 3a. Then the counter-form was filled with the mixture of dual-component silicone rubber and catalyst. By this way, the form to produce DCB specimens was fabricated, as shown in Fig 3b. Each of the two recesses had the following dimensions given in mm: 210 × 25 × 8.

To get the appropriate length and thickness of polymer, rectangular aluminum pieces thick on 4mm were placed between flat bars. The 3D model of a specimen taken out of the form is shown in Fig 4. After curing and 72-hour acclimatization aluminum pieces were removed.

Moreover, based on previously conducted preliminary examinations, besides pre-cracks the notches deep on 20–30 mm were additionally cut

Table 1. Polymer materials symbols and designations

Material symbol	Material designation
I	E53/Z1/100:10
II	E5/PAC/100:60
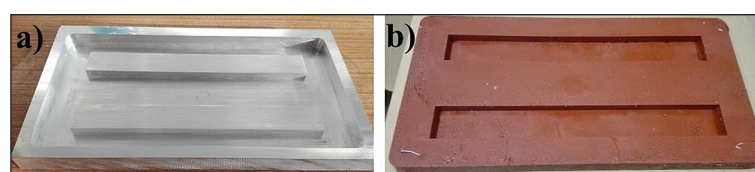
Figure 3. View of (a) the counter-form; (b) the form finally used for specimens preparation
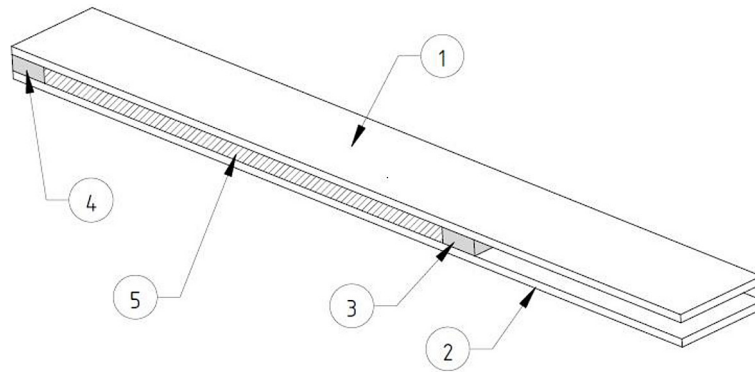
Figure 4. 3D model of a DCB specimen: 1 – top aluminum flat bar; 2 – bottom aluminum flat bar; 3 – front aluminum piece; 4 – rear aluminum piece; 5 – adhesive layer (cured epoxy resin)
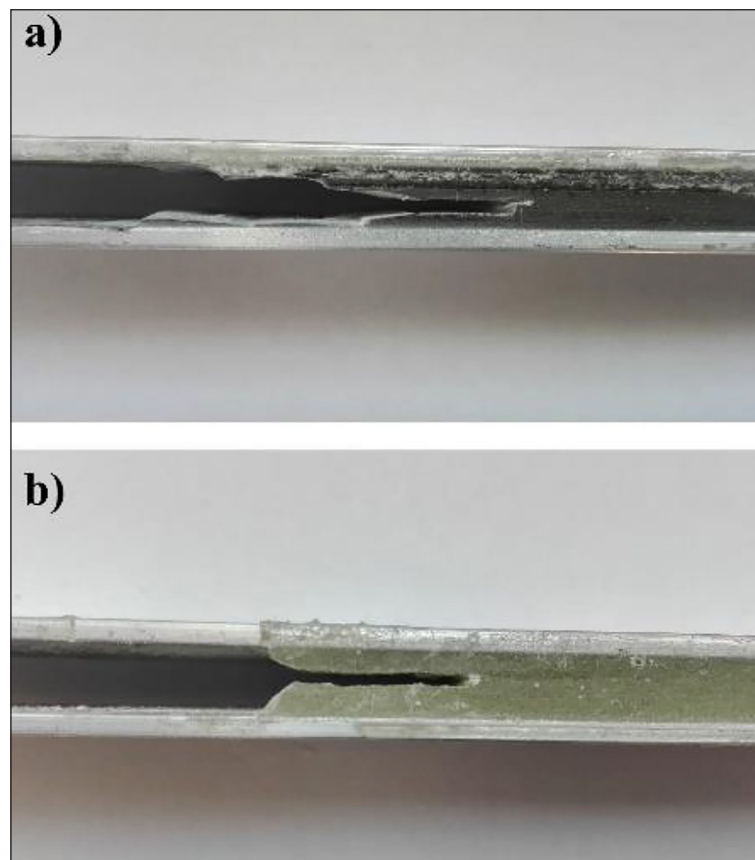
Figure 5. View of notches cut in DCB specimens: (a) material I; (b) material II

with emphasized deepening, as visible in Figure 5, to get a right direction of propagation. This way of specimen preparation induced that cracks propagated inside the polymer material as assumed. Previously taken examinations on specimens made of flat bars without sandblasting or with a notch cut not so deep as 20–30 mm proved that this way of preparation was not sufficient to make the crack goes right inside the polymer. Therefore, additional examination on aluminum flat bar surfaces was conducted to analyze surface parameters.

Surface analysis

In Fig. 6 the microscopic views of aluminum flat bars surfaces are presented. Keyence VHX-5000 with magnification of x500 was used to take the pictures. Three different types of top layer preparation were considered: no treatment, treatment using P150 sand paper and sandblasting. Fig. 6a shows a surface non modified while Figs 6b-c shows surfaces having a modified physisorptive layer. As it can be seen there are
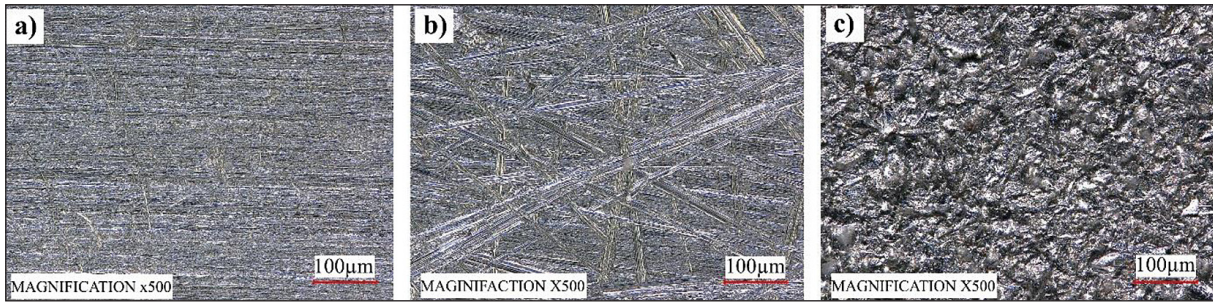
Figure 6. Microscopic view of flat bar surfaces: (a) no treatment, (b) after P150, (c) after sandblasting

characteristic machining traces depending on a treatment, which was applied to eliminate a top layer dirtiness.

Moreover, 3D T8000 RC-120-400 device produced by Hommel-Etamic which is generally used for measurement of contour, roughness and topography let to analyze the selected 2D and 3D roughness parameters of aluminum flat bars surfaces. Measuring tip with radius of 2 µm was used during the research. The following 3D roughness parameters were analyzed: Sq – root mean square value of the 3D profile datums, Sp – maximum 3D profile peak height and Sz – maximum 3D profile height. The isometric views of analyzed surfaces are shown in Figure 7. Based on the conducted research of selected roughness parameters and analysis of results it can be noticed that surface development is at appropriate level in the case of samples presented in Figures 7b–c. However, the right level of surface development is necessary to prepare the DCB specimens correctly. Influence of sandblasting treatment on geometrical development of the surface is significant. It was observed that all analyzed roughness parameters is five times higher than in case of surfaces with no treatment. Roughness parameters after sandblasting are as follows: Sq = 2.30 µm, Sp = 15.2 µm and Sz = 29.6 µm. However, it can be inferred that both coated abrasive tool and sandblasting

treatment let to eliminate dirtiness in physisorptive layer efficiently.

Furthermore, PGX goniometer equipped with dedicated software was used to determine surface free energy (SFE). All examinations took place at ambient temperature 19–21 °C and relative humidity 45–50%. Measurements of contact angle were conducted minimum ten times on every specimen using both water and diiodomethane. Firstly, measuring plate was checked horizontally by optical contour. Liquids used to determine contact angles were placed on the surfaces automatically by goniometer – as a drop with constant volume of 5 µl. For calculations the following values of surface free energy and its components were taken: water SFE γ_w = 72.8 mJ/m^2, polar component of water SFE γ^p_w = 51.0 mJ/m^2, dispersive component of water SFE γ^d_w = 21.8 mJ/m^2, diiodomethane SFE γ_d = 50.8 mJ/m^2, polar component of diiodomethane SFE γ^p_d = 2.3 mJ/m^2, dispersive component of diiodomethane SFE γ^d_d = 48.5 mJ/m^2. In Figure 8 some exemplary photos of measuring liquids used to determine contact angles and surface free energy. Moreover, mean values of contact angles for water and diiodomethane were presented for three types of flat bar surfaces. In Figure 9 surface free energy and its components (dispersive and polar) is shown for three different top layer preparation.
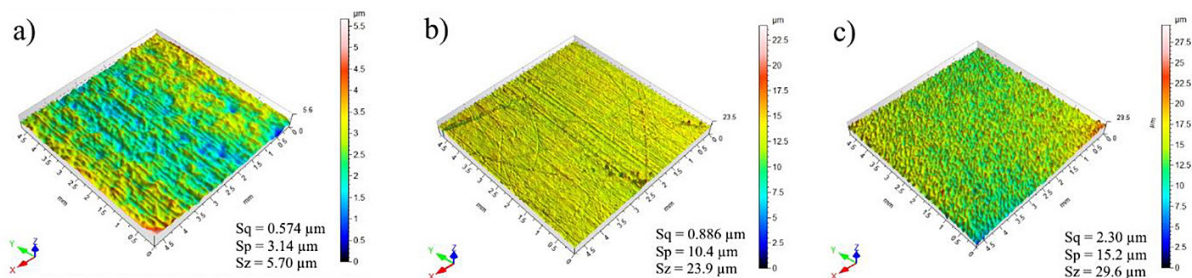
Figure 7. 3D contour diagrams of flat bar surfaces: (a) no treatment, (b) after P150, (c) after sandblasting; with three selected highness parameters given
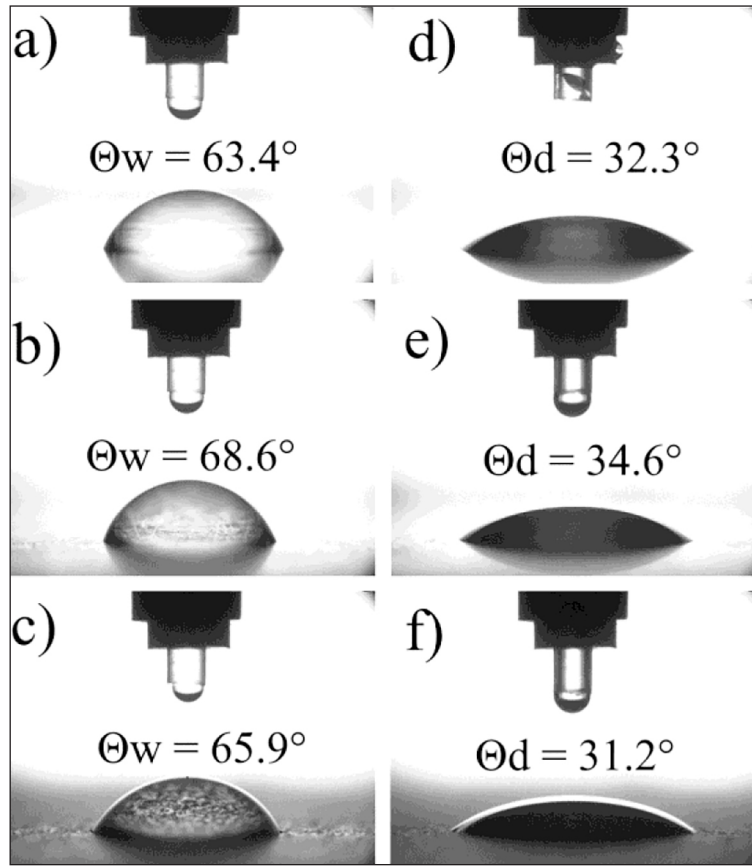
Figure 8. Mean values of contact angles for water: (a) no treatment, (b) after P150, (c) after sandblasting; mean values of contact angles for diiodomethane: (d) no treatment, (e) after P150, (f) after sandblasting
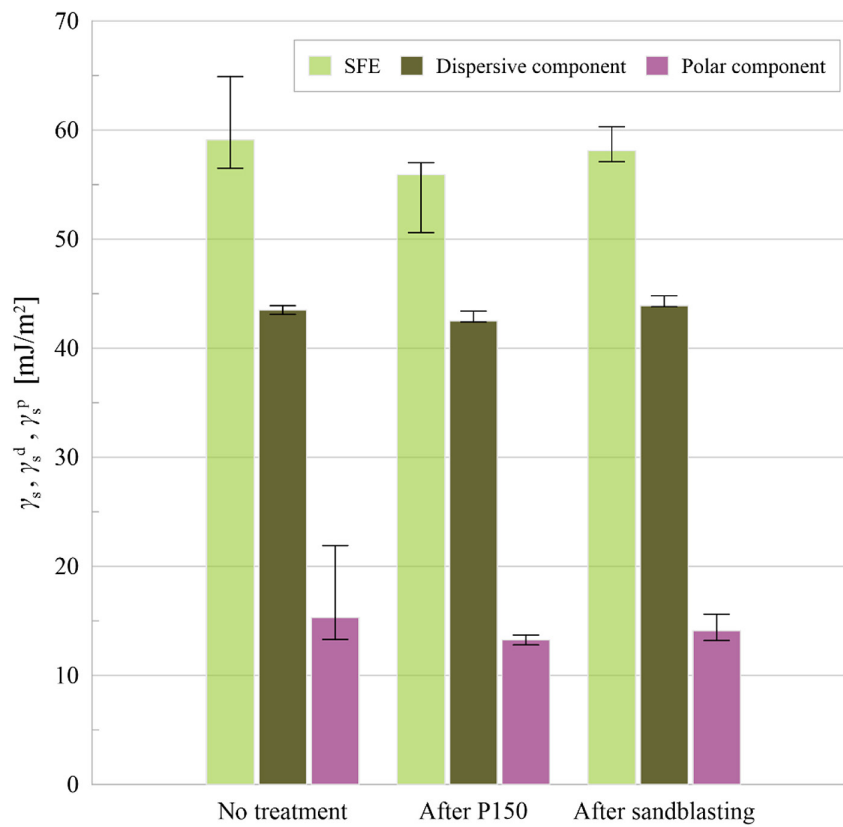
Figure 9. Surface free energy (SFE) for three types of flat bar preparation

Conducted analysis clearly proves that sandblasting treatment positively affects on a top layer energetic state of aluminum alloy. Mean value of surface free energy for all types of surface preparation is almost at the same level and equals to about 59 mJ/m². However, it is worth to notice that in comparison to other preparation methods, in the case of specimens after sandblasting treatment there is a lower scatter of results which is visible in a size of error bars. The lower the scatter of SFE results is the more homogeneous energetic state of the surface we have. It is one of the most necessary conditions in the case of adhesive technology.

In Figure 10 the selected 2D roughness parameters (Rz – maximum height of the roughness profile, Rt – total height of the profile) as well as SFE polar component are presented. As visible, mean value of SEF polar component is at the same level in all three cases and equals about 15 mJ/m². However, after coated abrasive tool (P150) and sandblasting treatment the scatter of results is much lower than in the case of no treatment. Values of roughness parameters are higher in the case of coated abrasive tool and sandblasting treatment while reach the highest values for specimens after sandblasting – almost eight times higher than in the case of no treatment specimens.

Higher roughness parameters values are advantageous for geometric surface development. Thus, above described analysis let to conclude that the best preparation method of aluminum flat bar is a sandblasting treatment.

Test procedure

DCB tests were conducted using the Autograph AGS-X 5kN universal testing machine manufactured by Shimadzu Corporation. Before the tests, piano hinges were bonded at both sites of each sample. Then, quasi-statical vertical loading was applied to DCB specimens with crosshead's speed equal to 1 mm/min. Currently, AMSY-5 system produced by Vallen Systeme GmbH was used to acquire acoustic emission parameters. The view of a loaded specimen for material I is presented in Figure 11. During examination the threshold was set to 0.05 mV (34 dB). All data was registered on computer's hard drive.

The AE system consisted of master unit equipped with ASIP-2 – 18-bit resolution analog to digital transducer with band width 1.6 kHz – 2.4 MHz and sampling frequency set to 10 MHz, AEP-4 pre-amplifier with 34 dB of gain and piezoelectric sensor 1045S manufactured by Fuji
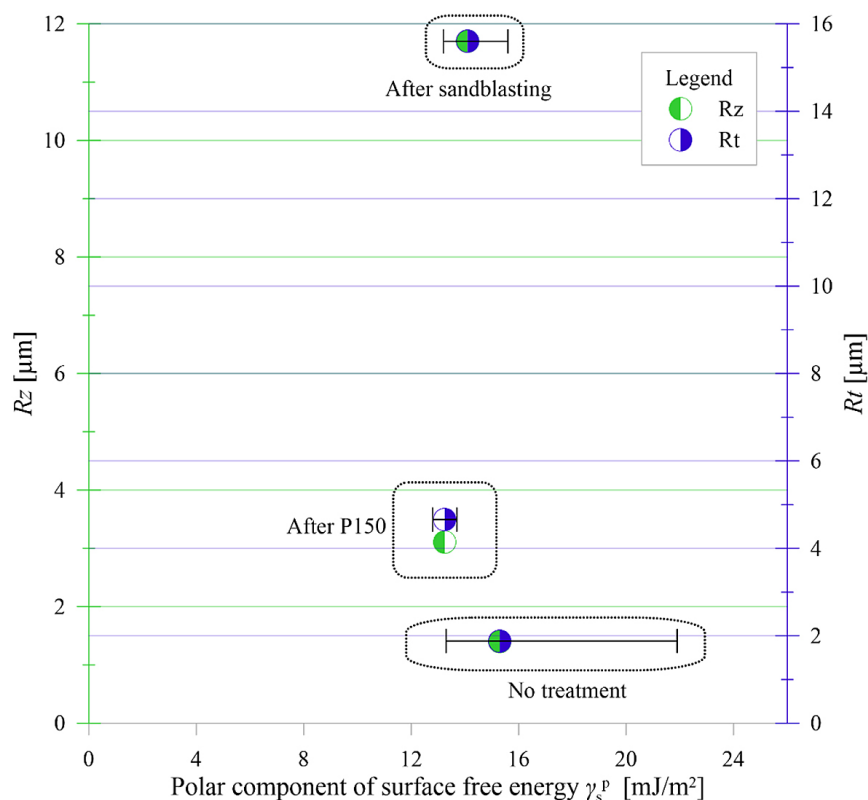
Figure 10. Polar component of surface energy versus two selected roughness parameters
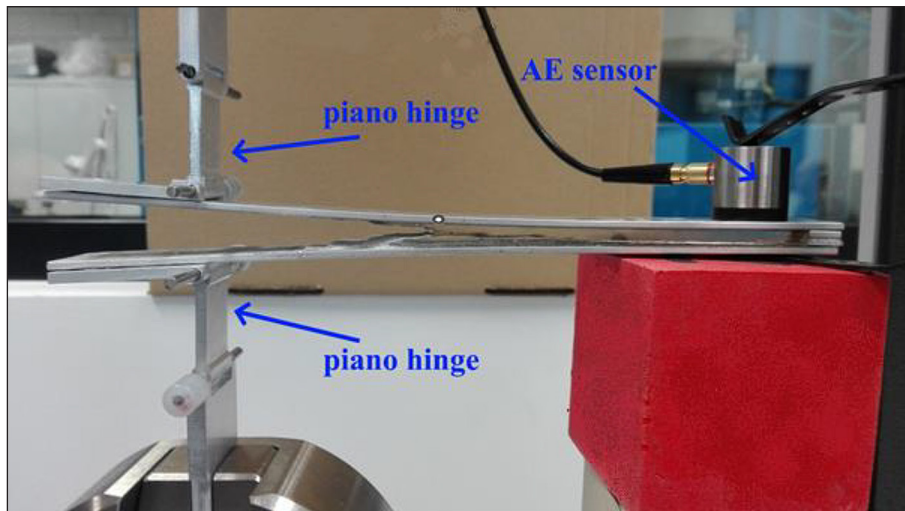
Figure 11. View of a loaded DCB specimen

Ceramics Corporation, which let to register the signal frequency up to 1.3 MHz. AE sensor was attached in 30 mm distance from sample's end. After the completion of data acquisition dedicated Vallen software was used to conduct the analysis.

RESULTS AND DISCUSSION

Based on the material properties of examined epoxies it was expected that fracture of DCB specimens would be brittle for the two material types. Although material II consisted of PAC curing agent is more compliant than material I, in all cases brittle fracture occured that happened suddenly and was accompanied by a loud fracture sound. Microscopic views analysis of fracture surfaces after the DCB test shows that there are some phenomena which are characteristic for brittle fructure: cracks going out of pores and so-called „river patterns", which are defined as ofsets on a cleavage plane. Single cracks were observed near the notch surface, whereas in the middle of a fracture surface „river patterns" appeared. Microscopic view of a fracture surface for material II is presented in Fig. 12.

During DCB tests hits, counts, amplitudes, frequencies (f_{AE}) as well as values of peak force (P_{MAX}) and corresponding energy (E_{AE}) were stored on computer's hard drive. In the next three figures (Figs. 13–15) mean values of energy and amplitude, number of hits and counts, as well as force and frequency were plotted, respectively. As it can be seen in Fig. 13 energy of emitted
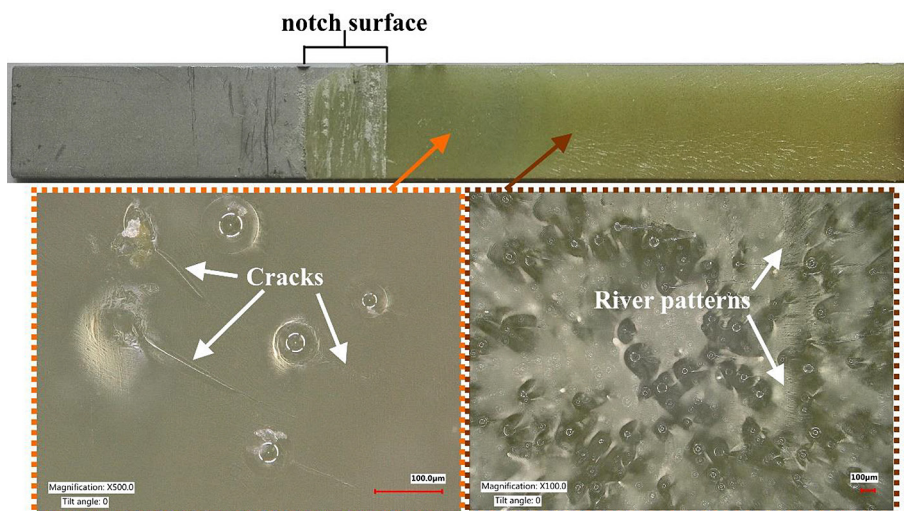
Figure 12. Microscopic view of a fracture surface after DCB test
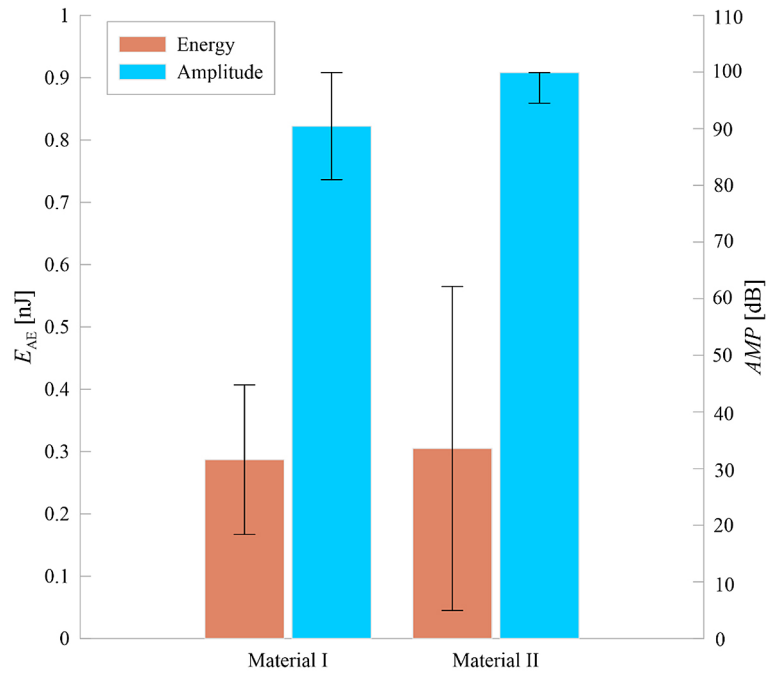
Figure 13. Mean values of AE energy and amplitude for the two tested materials
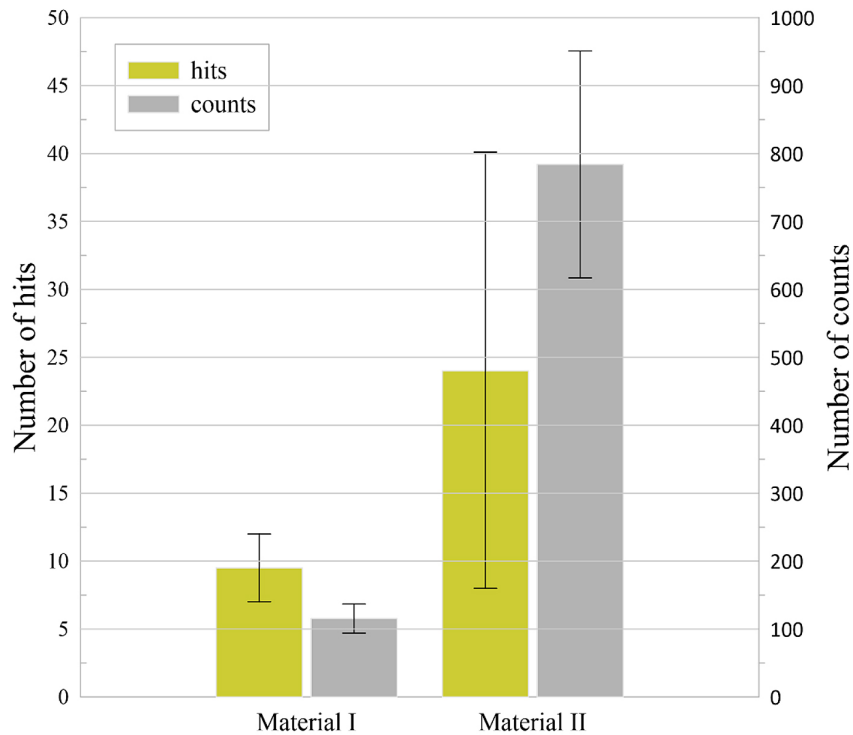
Figure 14. Mean values of hits and counts for the two tested materials

elastic waves was very small and comparable for both materials. Mean values of E_{AE} for material I and II were equal 0.287 nJ and 0.305 nJ, respectively. The scatter of E_{AE} results was quite high, however the full range of E_{AE} values for all samples did not exceed 0.6 nJ and were accurately in the range of 0.04–0.57 nJ. Moreover,

mean values of amplitude were also comparable in case of both tested materials and equal to 90.45 dB for material I and 99.9 dB for material II. It is worth to note that the amplitude value of 99.9 dB was the maximum value that could be registered by system. As it is presented in Fig. 14 mean value of number of hits and counts was

equal to 9.5 and 115.5 respectively for material I whereas it was equal to 24 and 784 for material II, respectively. It can be concluded that both parameters were much greater in the case of material II. The number of counts for material II was over five times of counts for material I. The number of hits for material II was about 150% greater than for material I.

Mean values of acoutic emission frequency versus maximum force were plotted in Fig. 15. As it is visible in the graph mean value of f_{AE} for material I and II was equal to 117.5 kHz and 45 kHz, respectively which means that the difference was of 2.6 times. Mean values of maximum force registered for material I and II were comparable and equal to 55.95 N and 63.7 N, respectively which means that no differences can be noticed based only on a force analysis. Based on the conducted analysis it can be concluded that each of the two tested materials presented different behavior in terms of emitted acoustic signals. However, the most reliable parameters seem to be hits, counts and acoustic emission frequency because in the case of them the differences between materials were the most visible as well as the scatter of results was very low in most cases. Hence, above mentioned parameters are better candidates to indetifying failure inside tested polymers and give

more accurate results than acoustic emission energy, amplitude and peak force which let to get an overall classification of the problem but without distinguishment to a particular material.

Based on data analysis of the results presented in Figs. 14–15 it can be concluded that number of both hits and counts were higher for material II in comparison to material II whereas AE frequency was lower for material II. Thus, the increase of hits and counts is related to a decrease of frequency. This is in a good agreement with authors' previously conducted research [34] on compact tension specimens made of the same epoxy materials. This proves that the results and described tendency represent material characteristics which does not depend on the testing method.

Furthermore, a WT tool was used to get some additional information on selected measurement points. An example of hit analysis in the case of specimen made of material II is presented in the next three graphs. Amplitude time-course is shown in Figure 16. It is visible that the hit lasted over 80 µs. In the figure threshold is indicated as horizontal lines at 0.05 mV. Moreover, the counts can be observed as a number of points when waveform crossed the treshold. Wavelet Transformation was applied to create diagrams of WT coefficients for material II
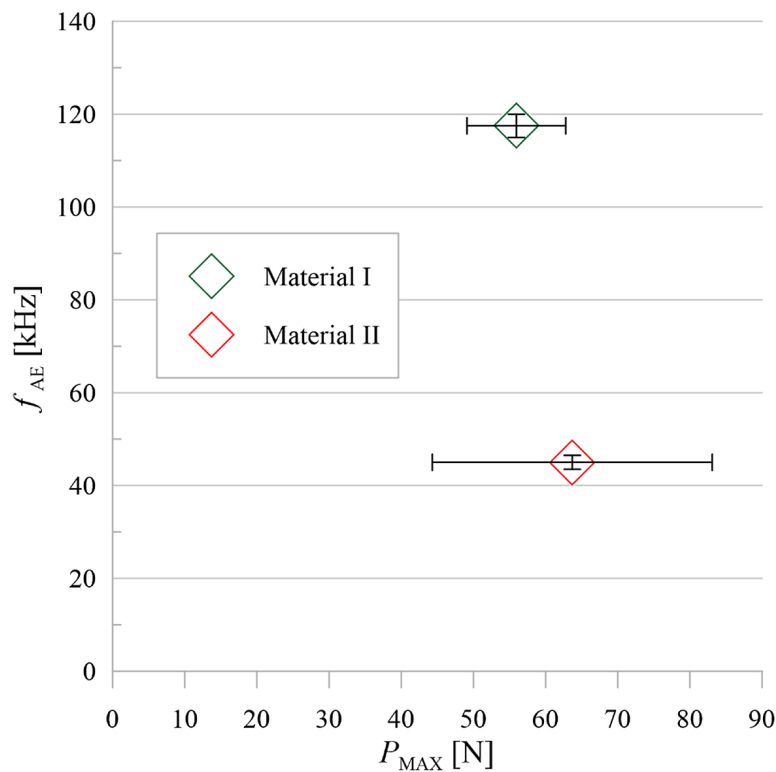
Figure 15. Mean values of maximum force and AE frequency for the two tested materials
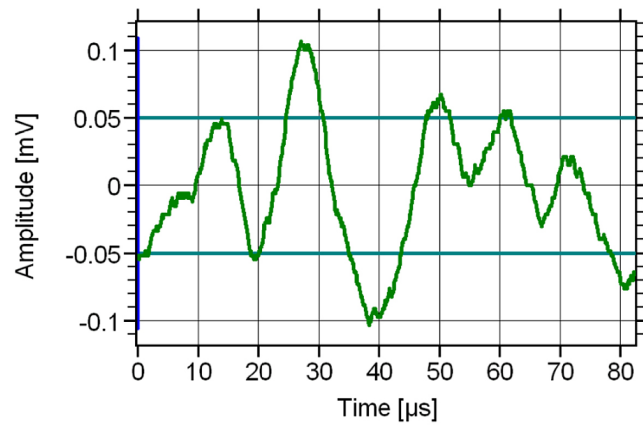
Figure 16. Amplitude timecourse for a hit
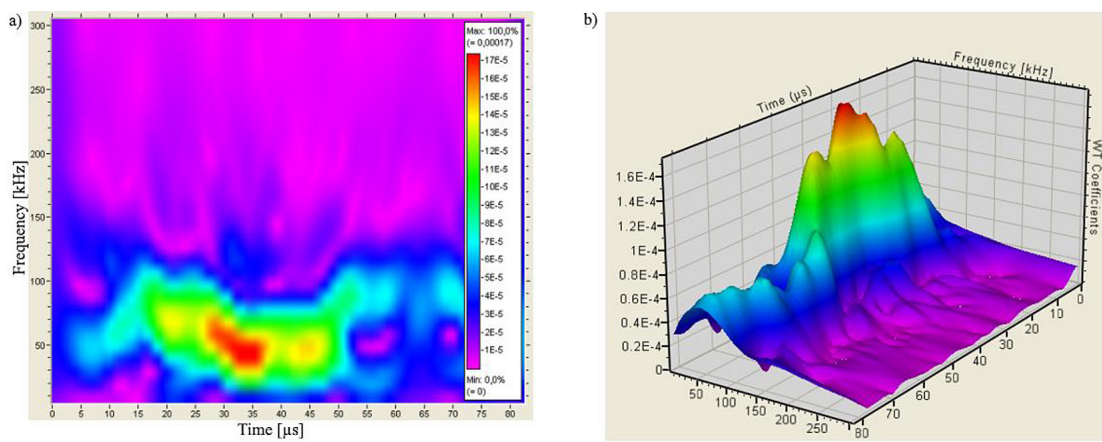
Figure 17. (a) Diagram of WT coefficients at linear scale; (b) 3D representation of WT coefficients
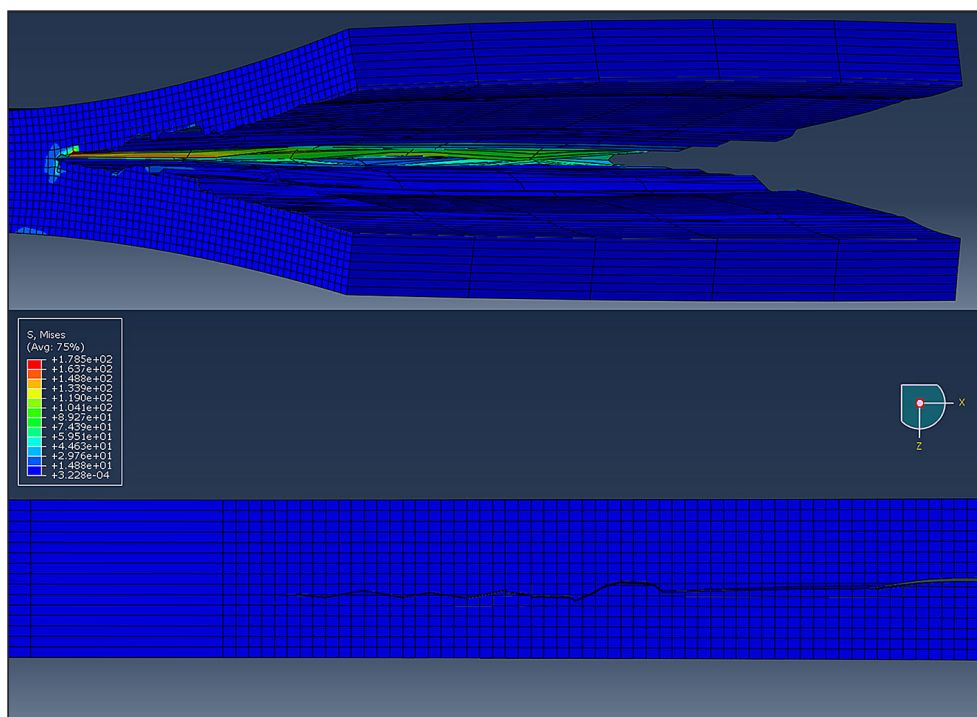
Figure 18. Numerical results for fracture analysis

specimen, as presented in Figure 17a by linear scale. It can be noticed that the time duration while the hit reaches peak frequencies started at 30 μs and lasted tens of μs. Moreover, in Figure 17b the 3D representation of WT coefficients is shown. It can be concluded that peak amplitude value taken from the FFT plot corresponds well with the color maps presented in Figure 17. Furthermore, numerical simulation of fracture was also conducted using a finite element method (FEM). Abaqus software version 2020 was employed and the material data of the adhesive material was based on the material tests presented in [35]. As for the specimen model, it consists of two stiffening elements and the test material between these elements. The two stiffening elements consist of 3400 C3D8R solid elements each. The adhesive material model was also made based on C3D8-type solid elements and with 5850 finite elements. In order to obtain a crack in the longitudinal symmetry plane of the element, the finite element mesh was densified in the area of failure initiation and propagation (Fig. 18). In addition, a crack initiation element was introduced to represent the notch cut (cf. Fig. 5). For the chosen material, the maximum force reached a value of nearly 46 N. The finite element mesh structure and the resultant crack are shown in Figure 18.

As it can be seen in the Figure 19, the numerical characteristic of the studied material is linear in the first phase, i.e. before reaching the maximum force. The maximum load is 60 N with the displacement of 0.34 mm, and it decreases until the total failure occurs. The consecutive drops in force values, after the peak value, represent small crack tip jumps. The sudden drop in force value is present at the displacement value of 0.44 mm which is accompanied by a significant crack length increase. After that, the force value is remarkably lower.
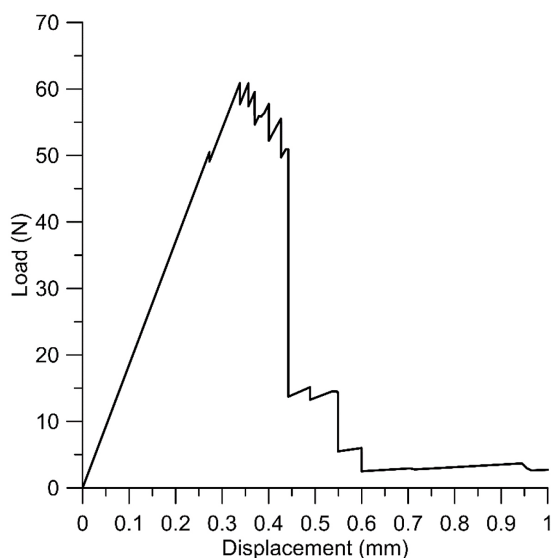
CONCLUSIONS

Based on the research it can be inferred as follows:

1. Acoustic emission used for damage monitoring of selected epoxies let to determine different results in case of each tested material whereas maximum forces registered were aproximately at the same level. Thus, this proves that acoustic emission is a valuable technique that let to obtain more comprehensive results than in the case of pure mechanical testing. Each of AE parameters registered during the test show that its value reacted to the material failure. However, hits, counts and AE frequency were distinguished as the ones giving the most accurate results in case of tested materials. Furthermore, these three parameters can help to relate the failure with a particular material because their values varied in case of material I and II, whereas other AE parameters had their results at comparable level for both materials.

2. Number of both hits and counts was higher in the case of more compliant material II (E5/PAC/100:60) in comparison to material I (E53/Z1/100:10) whereas AE frequency was lower in the case of material II. This trend observed after DCB test is in a good agreement with authors' previously conducted CT test. DCB test can be succesfully conducted not only to composite laminates but also to cured epoxy resin used as matrices in FRP composites. However, a special procedure is required to prepare specimens properly: flat bars surfaces which help to initiate the cracking goes inside the thick adhesive layer must be sandblasted that provides geometric surface development at demanding level. It was proved by analysis of roughness parameters and surface free energy.

3. Wavelet transform was found as a promising tool to localize frequency in time and it will be the aim of authors' further scientific research.

Figure 19. Force-displacement characteristic of resin DCB specimen

REFERENCES

1. Tabrizi IE, Kefal A, Zanjani JSM, Akalin C, Yildiz M. Experimental and numerical investigation on fracture behavior of glass/carbon fiber hybrid composites using acoustic emission method and refined zigzag theory. Composite Structures 2019; 223: 110971. https://doi.org/10.1016/j.compstruct.2019.110971

2. Aggelis DG, De Sutter S, Verbruggen S, Tsangouri E, Tysmans T. Acoustic emission characterization of damage sources of lightweight hybrid concrete beams. Engineering Fracture Mechanics 2019; 210: 181–8. https://doi.org/10.1016/j.engfracmech.2018.04.019

3. Seyyed Monfared Zanjani J, Saner Okan B, Yilmaz C, Menceloglu Y, Yildiz M. Monitoring the interface and bulk self-healing capability of tri-axial electrospun fibers in glass fiber reinforced epoxy composites. Composites Part A: Applied Science and Manufacturing 2017; 99: 221–32. https://doi.org/10.1016/j.compositesa.2017.04.017

4. Kubiak T, Samborski S, Teter A. Experimental investigation of failure process in compressed channel-section GFRP laminate columns assisted with the acoustic emission method. Composite Structures 2015; 133: 921–9. https://doi.org/10.1016/j.compstruct.2015.08.023

5. Haggui M, El Mahi A, Jendli Z, Akrout A, Haddar M. Static and fatigue characterization of flax fiber reinforced thermoplastic composites by acoustic emission. Applied Acoustics 2019; 147: 100–10. https://doi.org/10.1016/j.apacoust.2018.03.011

6. Ben Ameur M, El Mahi A, Rebiere J-L, Gimenez I, Beyaoui M, Abdennadher M, et al. Investigation and identification of damage mechanisms of unidirectional carbon/flax hybrid composites using acoustic emission. Engineering Fracture Mechanics 2019; 216: 106511. https://doi.org/10.1016/j.engfracmech.2019.106511

7. Barile C. Innovative mechanical characterization of CFRP by using acoustic emission technique. Engineering Fracture Mechanics 2019;210:414–21. https://doi.org/10.1016/j.engfracmech.2018.02.024

8. Rzeczkowski J, Samborski S, de Moura M. Experimental investigation of delamination in composite continuous fiber-reinforced plastic laminates with elastic couplings. Materials 2020; 13: 5146. https://doi.org/10.3390/ma13225146

9. Rzeczkowski J. An experimental analysis of the end-notched flexure composite laminates beams with elastic couplings. Continuum Mech Thermodyn 2020. https://doi.org/10.1007/s00161-020-00903-2

10. Barile C, Casavola C, Pappalettera G. Acoustic emission waveform analysis in CFRP under Mode I test. Engineering Fracture Mechanics 2019; 210: 408–13. https://doi.org/10.1016/j.engfracmech.2018.01.023

11. Berro Ramirez JP, Halm D, Grandidier J-C. Assessment of a damage model for wound composite structures by acoustic emission. Composite Structures 2019; 214: 414–21. https://doi.org/10.1016/j.compstruct.2019.01.093

12. Samborski S, Gliszczynski A, Rzeczkowski J, Wiacek N. Mode I interlaminar fracture of glass/epoxy unidirectional laminates. Part I: Experimental Studies. Materials 2019; 12: 1607. https://doi.org/10.3390/ma12101607

13. Samborski S. Numerical analysis of the DCB test configuration applicability to mechanically coupled Fiber Reinforced Laminated Composite beams. Composite Structures 2016; 152: 477–87. https://doi.org/10.1016/j.compstruct.2016.05.060

14. Kamiyama K, Mikuni M, Matsumoto T. Fracture propagation analysis on two component type acrylic adhesive joints. International Journal of Adhesion and Adhesives 2018; 83: 76–86. https://doi.org/10.1016/j.ijadhadh.2018.02.019

15. Yilmaz C, Akalin C, Gunal I, Celik H, Buyuk M, Suleman A, et al. A hybrid damage assessment for E-and S-glass reinforced laminated composite structures under in-plane shear loading. Composite Structures 2018; 186: 347–54. https://doi.org/10.1016/j.compstruct.2017.12.023

16. Gutkin R, Green CJ, Vangrattanachai S, Pinho ST, Robinson P, Curtis PT. On acoustic emission for failure investigation in CFRP: Pattern recognition and peak frequency analyses. Mechanical Systems and Signal Processing 2011; 25: 1393–407. https://doi.org/10.1016/j.ymssp.2010.11.014

17. Fotouhi M, Najafabadi MA. Acoustic emission-based study to characterize the initiation of delamination in composite materials: Journal of Thermoplastic Composite Materials 2014. https://doi.org/10.1177/0892705713519811

18. Vallen Systeme GmbH. AMSY-5 User Manual 2004.

19. Harčarik T, Bocko J, Masláková K. Frequency analysis of acoustic signal using the fast fourier transformation in MATLAB. Procedia Engineering 2012; 48: 199–204. https://doi.org/10.1016/j.proeng.2012.09.505

20. Fletcher P, Sangwine SJ. The development of the quaternion wavelet transform. Signal Processing 2017; 136: 2–15. https://doi.org/10.1016/j.sigpro.2016.12.025

21. Abdulkareem M, Bakhary N, Vafaei M, Noor NM, Mohamed RN. Application of two-dimensional wavelet transform to detect damage in steel plate structures. Measurement 2019; 146: 912–23. https://doi.org/10.1016/j.measurement.2019.07.027

22. Zhu L-F, Ke L-L, Zhu X-Q, Xiang Y, Wang Y-S. Crack identification of functionally graded beams using continuous wavelet transform. Composite Structures 2019; 210: 473–85. https://doi.org/10.1016/j.compstruct.2018.11.042

23. Skoczylas J, Samborski S, Kłonica M. The application of composite materials in the aerospace industry. Journal of Technology and Exploitation in Mechanical Engineering 2019; 5. https://doi.org/10.35784/jteme.73

24. Bielawski R, Rządkowski W, Kowalik MP, Kłonica M. Safety of aircraft structures in the context of composite element connection. International Review of Aerospace Engineering (IREASE) 2020; 13: 159–164. https://doi.org/10.15866/irease.v13i5.18805

25. Masiewicz J, Roszowska-Jarosz M, Kostrzewa M, Jasik A, Krawczyk P. The modification of an epoxy resin by natural plant materials 2020. https://doi.org/10.2478/oszn-2020-0003

26. Zheng T, Xi H, Wang Z, Zhang X, Wang Y, Qiao Y, et al. The curing kinetics and mechanical properties of epoxy resin composites reinforced by PEEK microparticles. Polymer Testing 2020; 91: 106781. https://doi.org/10.1016/j.polymertesting.2020.106781

27. Wu T, Liu Y, Li N, Huang G-W, Qu C-B, Xiao H-M. Cryogenic mechanical properties of epoxy resin toughened by hydroxyl-terminated polyurethane. Polymer Testing 2019; 74: 45–56. https://doi.org/10.1016/j.polymertesting.2018.11.048

28. Kubit A, Trzepiecinski T, Kłonica M, Hebda M, Pytel M. The influence of temperature gradient thermal shock cycles on the interlaminar shear strength of fibre metal laminate composite determined by the short beam test. Composites Part B: Engineering 2019; 176: 107217. https://doi.org/10.1016/j.compositesb.2019.107217

29. Wang RM, Zheng SR, Zheng YG. Polymer Matrix Composites and Technology. Beijing. China: Woodhead Publishing; 2011.

30. Kłonica M. Impact of thermal fatigue on young's modulus of epoxy adhesives. Advances in Science and Technology Research Journal 2015; 9: 103–6. https://doi.org/10.12913/22998624/60795

31. Jin F-L, Li X, Park S-J. Synthesis and application of epoxy resins: A review. Journal of Industrial and Engineering Chemistry 2015; 29: 1–11. https://doi.org/10.1016/j.jiec.2015.03.026

32. ASTM D5528-13, Standard test method for mode i interlaminar fracture toughness of unidirectional fiber-reinforced polymer matrix composites, ASTM International, West Conshohocken, PA, 2013, www.astm.org n.d.

33. Rządkowski W, Tracz J, Cisowski A, Gardyjas K, Groen H, Palka M, Kowalik M. Evaluation of bonding gap control methods for an epoxy adhesive joint of carbon fiber tubes and aluminum alloy inserts. Materials 2021; 14(8): 1977; https://doi.org/10.3390/ma14081977

34. Skoczylas J, Kłonica M, Samborski S. A study on the FRP composite's matrix damage resistance by means of elastic wave propagation analysis. Composite Structures 2022; 297: 115935. https://doi.org/10.1016/j.compstruct.2022.115935

35. Skoczylas J, Samborski S, Kłonica M. A multilateral study on the FRP Composite's matrix strength and damage growth resistance. Composite Structures 2021; 263: 113752. https://doi.org/10.1016/j.compstruct.2021.113752